Chapter

Enhanced Nonlinear PID Controller for Positioning Control of Maglev System

Shin-Horng Chong, Roong-Soon Allan Chan and Norhaslinda Hasim

Abstract

Magnetic levitation (maglev) is a way of using electromagnetic fields to levitate objects without any noise or the need for petrol or air. Due to its highly nonlinear and unstable behavior, numerous control solutions have been proposed to overcome it. However, most of them still acquire precise dynamic model parameters, or deep understanding of control theory. To account the complexity in the design procedure, a practical controller consists of classical and modern control approaches are proposed. This chapter presents a practical controller for high positioning performance of a magnetic levitation system. Three strategies of the proposed controller where the PI-PD controller is to enhance transient response, the model-based feedforward control (FF) is incorporated with the PI-PD controller to enhance the overshoot reduction characteristic in attaining a better transient response, and lastly the disturbance compensator (K_z) is integrated as an additional feedback element to reduce the sensitivity function magnitude for robustness enhancement. The proposed controller - FF PI-PD + K_z has a simple and straightforward design procedure. The usefulness of the proposed controller is evaluated experimentally.

Keywords: maglev system, disturbance compensator, model-based feedforward control, PI-PD control, robustness

1. Introduction

Magnetic levitation (maglev) system produces an electromagnetic force as the electric current flow through the coils to support a levitated object. This indicates that the maglev system eliminates the mechanical contact and friction between the moving and stationary parts. Due to the advantages, the maglev system has been successfully and widely implemented for many high-speed motion applications such as the high-speed maglev passenger trains, magnetic bearing system, flywheel energy storage system and vibration isolation system [1]. However, the maglev system is open loop instability and inherent nonlinearities. In addition, it is a non-damping system which has fast response, yet sensitive to vibration. Therefore, it remains a challenging task to design a feedback controller for attaining a good positioning performance in the maglev system.

Although a lot of advanced control strategy has been proposed for controlling maglev system, the classical controllers such as proportional integral derivative

(PID) and lead–lag compensators still are regularly employed in the industrial applications due to their simple structure, straightforward design procedure and easy to implement. In the past, a lead compensator [2] and cascaded lead compensation scheme [3] were designed to stabilize the maglev system. However, the classical controllers can only perform well in limited operating range and failed to demonstrate a satisfactory robustness performance. Thus, many advanced controllers such as feedback linearization [4], sliding mode control [5], H_∞ control technique [6], disturbance observer control approach [7], adaptive robust backstepping method [8] and model predictive control [9–11] as well as intelligent controllers which include fuzzy logic control [12] and neural network [13] have been dedicated to procure the high positioning and robustness performances in the maglev system. Despite the good positioning and robustness performances of the advanced controllers, sufficient knowledge of control theory is strictly needed in the design procedure. Furthermore, the intelligent controllers consist of complex architecture require a high computational effort. Often, the intelligent controllers do not have any systematic design procedure. These drawbacks depict barrier to their practical use.

Due to the above-mentioned reason, researchers kept devoting their effort in enhancing control performance of classic control in maglev system. The problem associated with 1-DOF PID control was overcome with the proposed of modified PID control and/or 2-DOF PID control. In 2007, Leva and Bascetta in [14] have realized a model-based feedforward control to the PID controller to improve the tracking performance of a maglev system. Unfortunately, it still demonstrated huge spike occurrence when the ball started moving at the initial position. After few years, Ghosh et al. has proposed a 2-DOF PID controller to improve the system transient response with zero percentage of overshoot. However, the proposed controller suffered from long settling time which was around 2 s. Besides, its positioning accuracy was recorded poor due to the derivative action on the reference signal [15]. In order to solve the positioning accuracy, Allan et al. has introduced the 2-DOF Lead-plus-PI controller [16]. The experimental evidence reported the improvement in the positioning accuracy, yet to point-to-point motion performance was deteriorated as the levitation height was increased.

Thus, in this research, a proportional integral-proportional derivative control with feedforward and disturbance compensations (FF PI-PD + K_z) control approach is proposed to stabilize the maglev system and enhance the positioning performance as well as its robustness. The proposed controller consists of a PI-PD controller, a model-based feedforward control and a disturbance compensator. The PI-PD controller is designed by using the pole-placement method; the model-based feedforward control is constructed based on the system driving characteristic in open loop; the disturbance compensator is developed via the system current dynamics in closed loop. The derivative action of the PI-PD control amplified the measurement noise that affected the positioning accuracy. Hence, a low pass filter is featured with the PI-PD control to suppress the bad influence of the derivative action. Besides, a model-based feedforward control is incorporated with the PI-PD controller to further improve the following characteristic of the mechanism in attaining a better overshoot reduction characteristic. At the same time, the positioning time is greatly reduced. Lastly, a disturbance compensator is integrated as an additional feedback element for robustness enhancement via lowering the sensitivity function magnitude. The effectiveness of the FF PI-PD + K_z controller is validated experimentally through two types of motion control that are point-to-point and tracking motions. In this present paper, the robustness of the FF PI-PD + K_z controller is examined via applying an impulse disturbance and varying the mass. The positioning and robustness performances of the FF PI-PD + K_z controller are compared with the FF PI-PD and the full state feedback (FSF) controllers.

The remainder of this chapter is outlined as follow. In Section 2, the experimental setup and mathematical modeling of the maglev system are represented. Section 3 explains the control structure, design procedure and stability analysis of the FF PI-PD + K_z controller. In Section 4, the experimental results are discussed. Lastly, the conclusion is drawn in Section 5.

2. Experimental setup and dynamic modeling

This section presents the experimental setup and dynamic modeling of the maglev system.

2.1 Experimental setup

The single-axis maglev mechanism (Googoltech GML 2001), as shown in **Figure 1** is used as a testbed to clarify the usefulness of the proposed controller. The maglev system is only able to control object to move up and down. The control purpose is to keep the magnetic levitation ball stable in a given position or to make the ball track a desired trajectory.

The maglev mechanism consists of an electromagnet (number of windings, N_w = 1000 turns) to exert a tractive force across the air gap to levitate a steel ball (mass, M = 94 g). Besides, it is a voltage-controlled (control signal, u = 0–10 V) maglev mechanism, which is comprised of a power amplifier to actuate the electromagnet. The maximum electrical power consumption is around 16 W. The maximum levitation height of the maglev system is 15 mm. In the experiments, the initial position is set at 10.5 mm and the operating range is within ±2.5 mm. A laser position sensor (Panasonic laser distance sensor HG-C1050) with resolution of 1.83 μm is used to measure the levitation displacement. As experimentally examined, the resolution of the laser sensor output in open loop is recorded at 15 μm. To measure the controlled current of the mechanism, a hall effect current sensor

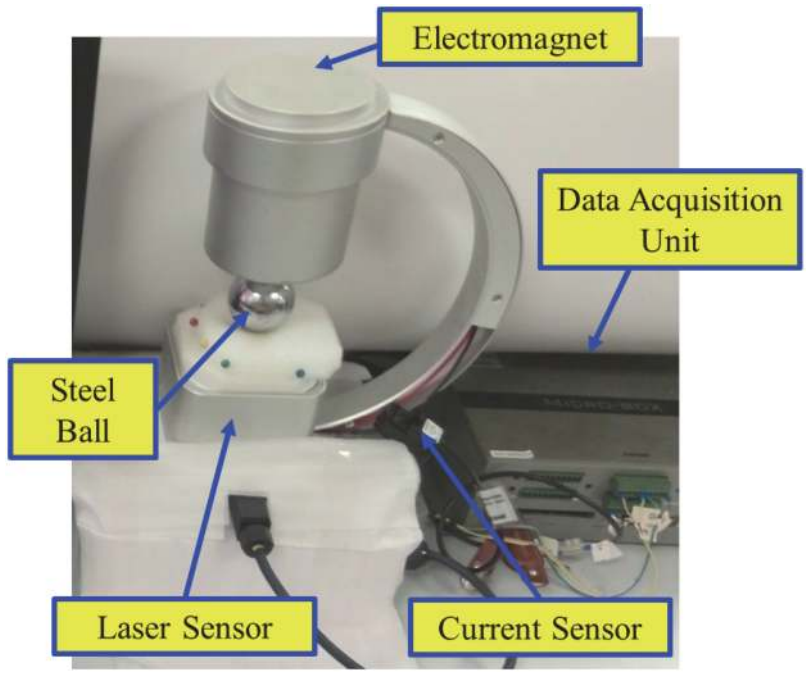

Figure 1.
Maglev system.

(Magnelab hall effect current sensor HCT-0010-005) with resolution of 0.38 mA is used. The controller is implemented at a sampling rate of 1 kHz.

2.2 Dynamic modeling

Figure 2 illustrates the principle diagram of maglev system. The dynamic equation of the maglev system is

$$M\frac{d^2x}{dt^2} = -F_m(i,x) + F_g \tag{1}$$

where M, F_{m}, F_g, i and x denote the steel ball mass, electromagnetic force, gravitational force, current and levitation height respectively.

The F_m (i, x) is in negative sign indicates that it always functioning in opposite direction against the gravitational force, F_g.

The electromagnetic force, $F_m(i, x)$ is described as

$$F_m(i,x) = K\frac{i^2}{x^2} \tag{2}$$

where K represents the electromagnetic constant.

The gravitational force, F_g is denoted as

$$F_g = Mg \tag{3}$$

where g represents the gravitational acceleration.

Substitute Eqs (2) and (3) into Eq. (1), the dynamic equation of the maglev system can be accordingly rewritten as

$$\frac{d^2x}{dt^2} = -\frac{K}{M}\frac{i^2}{x^2} + g \tag{4}$$

The Eq. (2) shows the inherent nonlinearities characteristic of the F_m (i, x) which can be linearized by using the Taylor Series approximation at the equilibrium position where

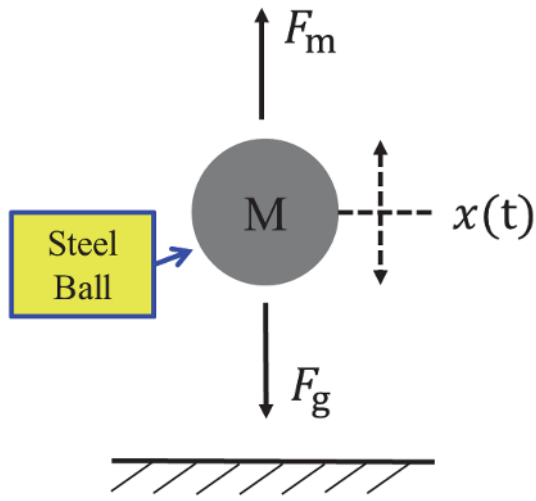

Figure 2.
The principal diagrams of the maglev system.

$$F_m(i,x) \approx F_m(i_o,x_o) + \frac{\partial F_m(i,x)}{\partial i} i(t) + \frac{\partial F_m(i,x)}{\partial x} x(t) \tag{5}$$

During levitating, the relationship between the $F_m\ (i, x)$ and the F_g is governed by

$$M_g = F_m(i_o,x_o) \tag{6}$$

where i_o and x_o denote the nominal current and nominal displacement, respectively.

Substitute Eqs (5) and (6) into Eq. (1), and undergoes Laplace transform on Eq. (1), the linear transfer function is

$$\frac{X(s)}{I(s)} = \frac{-\frac{K_c}{M}}{\left[s^2 - \frac{K_x}{M}\right]} \tag{7}$$

where K_c and K_x represent the current and position coefficient, while X(s) and I(s) denote the levitation height and current, respectively, where $K_c = 2Ki_o/\ x_o^{\ 2}$ and $K_x = 2Ki_o^{\ 2}/x_o^{\ 3}$.

Rewrite Eq. (7) by involving power amplifier gain, K_a and sensor sensitivity gain, K_s, it becomes

$$G_p(s) = \frac{V_s(s)}{V_i(s)} = \frac{-\frac{K_s}{K_a}\frac{K_c}{M}}{\left[s^2 - \frac{K_x}{M}\right]} \tag{8}$$

The Eq. (8) is amplified to

$$G_p(s) = \frac{\beta}{s^2 - \gamma^2} \tag{9}$$

where $\beta = -K_sK_c/K_aM$ and $\gamma^2 = K_x/M$.

As shown in Eq. (9), it proves that the uncompensated system is unstable in open loop because it comprises of one pole located at the right half s-plane. Thus, a feedback control system is a vital need to stabilize the system. The system parameter values are shown in **Table 1**.

3. Proportional integral-proportional derivative control with feedforward and disturbance compensations (FF PI-PD + *K*z) control system framework

This section is devoted to explaining the formulation of FF PI-PD + K_z control approach for the maglev system. Next, the control strategy of FF PI-PD + K_z controller is discussed and followed by the design procedure of the proposed control. Lastly, the stability of the proposed control is examined.

3.1 Control structure

The block diagram of FF PI-PD + K_z control system for positioning and robust control of 1-DOF maglev system is depicted in **Figure 3**. The feedback loop consists of PI-PD control and disturbance compensation scheme, whereas the feedforward loop contains a model-based feedforward control. The FF PI-PD + K_z control system

Symbol	Description, unit	Value
M	Steel ball mass, Kg	9.40×10^{-2}
x_o	Nominal displacement, m	1.00×10^{-2}
i_o	Nnominal current, A	3.94×10^{-1}
K	Electromagnetic constant, Nm^2/A^2	2.31×10^{-4}
K_a	Power amplifier gain, V/A	6.51
K_s	Sensor sensitivity, V/m	1.67×10^2
g	Gravitational acceleration, m/s^2	9.81

Table 1.
Model parameters.

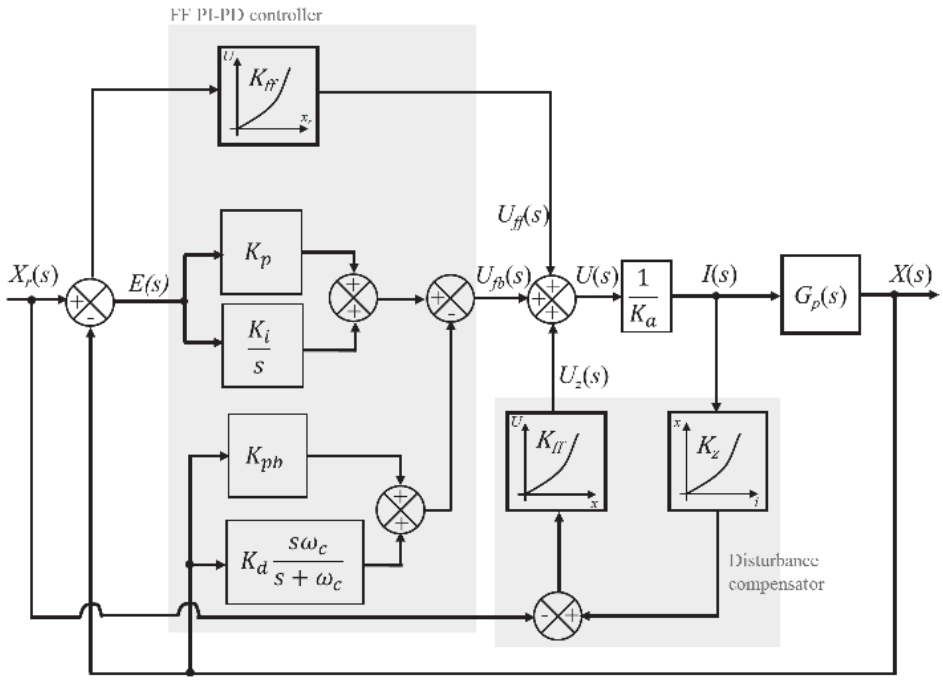

Figure 3.
Block diagram of the FF PI-PD + Kz control system.

is designed under the following considerations: (i) the PI-PD control is designed to improve the transient response of the conventional PID controller, (ii) the model-based feedforward control is integrated to obtain a better overshoot reduction characteristic and (iii) the disturbance compensation control is employed for robustness enhancement.

To design the FF PI-PD + K_z controller, the PI-PD control is designed at the first place. The PI-PD controller is proposed to improve the positioning performance of the conventional PID controller [17]. By moving the derivative action and some portion of the proportional gain to the feedback path, the resonance peak of conventional PID controller in the closed-loop frequency response can be reduced. Thus, it explains that the PI-PD controller demonstrates a better transient response than the conventional PID controller. Then, a low pass filter is adopted to improve the positioning accuracy by attenuating the amplification of the measurement noise. However, the PI-PD control transient response is unsatisfied because the overshoot remains high. To solve this problem, a model-based feedforward control is

incorporated with the PI-PD control to enhance the system following characteristic. This improvement leads to a better overshoot reduction characteristic and shorten the positioning time. Lastly, a disturbance compensator is introduced for robustness enhancement of the FF PI-PD control. The proposed disturbance compensator estimates the disturbances and imparts an adequate voltage to compensate them. Overall, the proposed FF PI-PD + K_z control system provides the advantages which are: (i) a better overshoot reduction characteristic; and (ii) low sensitivity to external disturbance and parameter variation.

The control law of the FF PI-PD + Kz control system is

$$U(s) = \left(K_p + \frac{K_i}{s}\right)E(s) - \left(K_{pb} + K_d\frac{s\omega_c}{s+\omega_c}\right)X(s) + K_{ff}X_r(s) + K_{ff}[K_zI(s) - X_r(s)] \tag{10}$$

where K_p, K_i, K_{pb}, K_d, K_{ff}, K_z, ω_c, *and* X_r denote the proportional gain, integral gain, feedback proportional gain, derivative gain, linearized feedforward gain, linearized disturbance compensator gain, system cut-off frequency and reference input, respectively.

3.2 Design procedure

There are three (3) major parts in the design procedure of the FF PI-PD + Kz control system.

3.2.1 PI-PD controller

The PI-PD controller is a modified PID controller, where it consists of derivative gain, K_d and some portion of the proportional gain, K_{pb} at the feedback path. Both are evidenced to have an approximately similar closed loop characteristic equation, as proved in Eqs (11) and (12).

$$\delta_{PID}(\mathrm{s}) = s^3 + \beta K_d s^2 + \left(K_p\beta - \gamma^2\right)s + K_i\beta \tag{11}$$

$$\delta_{PI-PD}(s) = s^3 + \beta K_d s^2 + \left[\left(K_p + K_{pb}\right)\beta - \gamma^2\right]s + K_i\beta \tag{12}$$

The desired characteristic equation of a general second-order system is denoted as

$$\delta_{desired}(s) = (s + \alpha\zeta\omega_n)\left(s^2 + 2\zeta\omega_n s + {\omega_n}^2\right) \tag{13}$$

where β, γ, α, ζ and ω_n represent the open loop gain, open loop pole, third pole location, desired damping ratio and desired natural frequency, respectively.

By comparing Eqs (11) and (13), the PID parameters (K_p, K_i and K_d) are

$$K_p = \frac{2\alpha{\omega_n}^2\zeta^2 + {\omega_n}^2 + \gamma^2}{\beta} \tag{14}$$

$$K_i = \frac{\alpha{\omega_n}^3\zeta}{\beta} \tag{15}$$

$$K_d = \frac{2\zeta\omega_n + \alpha\zeta\omega_n}{\beta} \tag{16}$$

To achieve a fast positioning with low overshoot performance, the design specifications are set as: settling time, t_s = 0.5 s, percentage of overshoot, $\%OS < 10\%$ and

third pole location, α = 10. After calculated the PID controller parameters, the derivative gain, K_d and some portion of the proportional gain, K_p are moved to the feedback path for acquiring the PI-PD control in enhancing the transient response. Even though both PI-PD and conventional PID controllers show an approximately similar closed loop characteristic equation, both of them comprised of different control law

$$U_{PID}(s) = \left(K_p + \frac{K_i}{s} + K_d s\right)E(s) \tag{17}$$

$$U_{PI-PD}(s) = \left(K_p + \frac{K_i}{s}\right)E(s) - \left(K_{pb} + K_d s\right)X(s) \tag{18}$$

Based on Eqs (17) and (18), the conventional PID controller is functioned based on the error signal, $E(s)$ only, whereas the PI-PD controller is operated based on the error signal, $E(s)$ and the output signal $X(s)$. Hence, the PI-PD controller tends to act faster than the conventional PID controller to compensate the error.

3.2.2 Model-based feedforward control

The model-based feedforward control is employed to improve the overshoot reduction characteristic of the PI-PD control. The control law of the model-based feedforward control is expressed as

$$U_{ff}(s) = K_{ff}X_r(s) \tag{19}$$

where K_{ff} and $X_r(s)$ represent the linearized feedforward gain and reference input.

From Eq. (19), the model-based feedforward control is acted based on the desired output or reference input. Hence, by using the feedforward control, the desired output is known in advance and it can synthesize an adequate control signal to the closed loop system for moving the mechanism to the targeted output. Thus, the model-based feedforward control is used to enhance the system following characteristic and provide a better overshoot reduction characteristic. It also leads to a faster positioning time.

To design the model-based feedforward control, the relationship between the controlled voltage and the levitation displacement is obtained via experiments. First, a ramp input voltage with gradient, m = 0.1 V/t is applied to the system at different levitation displacement from 0 mm to 15 mm with every 1 mm incremental displacement. Then, the minimum voltage to levitate the steel ball at various displacements is determined. The quantitative comparisons of ten (10) repeatability

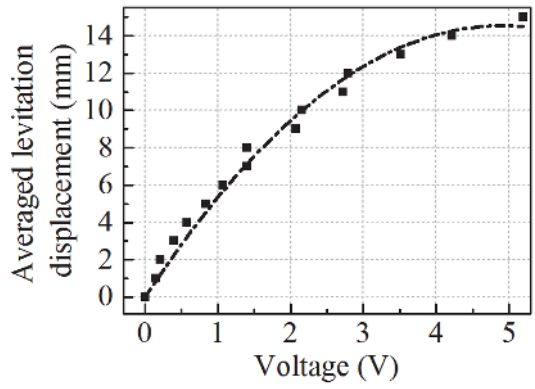

Figure 4.
The maglev system driving characteristic in open loop.

tests are carried out at various levitation displacements. **Figure 4** depicts the system driving characteristic that is measured and adopted as a model-based feedforward control in the proposed controller.

Figure 5 shows the step responses of the PI-PD and FF PI-PD controllers at 0.5 mm and 1.0 mm step inputs. In contrast to the PI-PD controller, the FF PI-PD controller demonstrates a better overshoot reduction characteristic. Besides, the FF PI-PD controller positioning time is shorter than the PI-PD controller. The comparative experimental performances show that the model-based feedforward control improves the overshoot reduction characteristic.

3.2.3 Disturbance compensator

In order to enhance the disturbance rejection characteristic of the proposed controller, a disturbance compensator is designed and incorporated with the FF PI-PD control, via lowering the magnitude of sensitivity function. In practical, the external disturbance and parameter uncertainties are lumped as an equivalent disturbance. A simple way to attenuate the equivalent disturbance is through introducing a cancelation term to it. The proposed disturbance compensator considers the difference between the actual output and the reference input as an equivalent disturbance. Then, an adequate voltage is applied to suppress the equivalent disturbance. The control law of the disturbance compensator is expressed as

$$U_z(s) = [X(s) - X_r(s)]K_{ff} \tag{20}$$

where $X(s) = K_z I(s)$, K_{ff}, K_z, $X(s)$ and $X_r(s)$ represent the linearized feedforward gain, linearized disturbance compensator gain, levitation height and reference input.

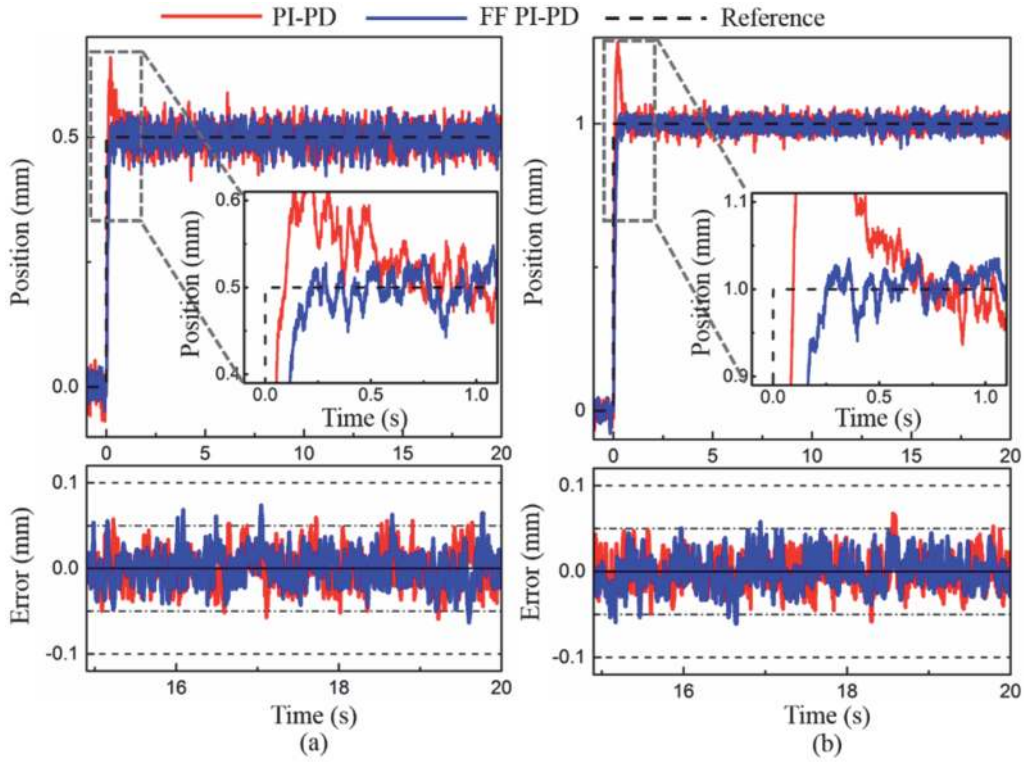

Figure 5.
Experimental step responses of the FF PI-PD and PI-PD control system. (a) Responses to a 0.5 mm step input. (b) Responses to a 1.0 mm step input.

From Eq. (20), the difference between the actual output and the reference input is considered as an estimated disturbance. Then, a sufficient voltage is applied to the control signal to attenuate the estimated disturbance.

To design the disturbance compensator, the relationship between the controlled current and the levitation displacement is attained experimentally. First, the mechanism is stabilized by a control system. Next, the required current to levitate the steel ball at different levitation displacement from −2.5 mm to 2.5 mm with every 0.5 mm interval displacement is measured. The quantitative comparisons of ten (10) repeatability tests are conducted at various levitation displacements. **Figure 6** shows the system current dynamic where 0 mm denotes the system datum or initial position which is at 10.5 mm. The system current dynamic is employed as a disturbance compensator in the proposed controller.

Figure 7 depicts the experimental impulse disturbance rejection performance of the FF PI-PD and FF PI-PD + K_z controllers. It can be seen clearly that the FF PI-PD + K_z controller is less sensitive to the external disturbance. The disturbance rejection characteristic of the FF PI-PD + K_z controller is proven theoretically by using the closed loop sensitivity function. The sensitivity functions of the FF PI-PD and FF PI-PD + K_z controllers are

$$S_{FFPI-PD}(s) = \frac{1}{1 + \left(K_p + \frac{K_i}{s} + K_{pb} + K_d \frac{s\omega_c}{s+\omega_c}\right) G_p(s)} \tag{21}$$

$$S_{FFPI-PD+K_z}(s) = \frac{1}{\left(K_a - K_{ff} K_z\right) + \left(K_p + \frac{K_i}{s} + K_{pb} + K_d \frac{s\omega_c}{s+\omega_c}\right) G_p(s)} \tag{22}$$

From Eqs (21) and (22), the proposed controller consists of the additional elements to reduce sensitivity of the system and hence to accomplish better robustness to disturbance. **Figure 8** presents the frequency responses of the FF PI-PD and FF PI-PD + K_z from the disturbance to the displacement. To decrease the effect of disturbance, the sensitivity functions of the closed-loop system must have sufficiently low magnitude. As can be seen clearly in **Figure 8**, the proposed controller consists of lower sensitivity magnitude than the FF PI-PD controller up to the range of 70 Hz. Thus, it can be expressed that the disturbance compensation control scheme of the proposed controller tends to improve the system disturbance rejection characteristic. In short, the FF PI-PD + K_z control system is less sensitive to the external disturbance and parameter variation in comparison to the FF PI-PD controller.

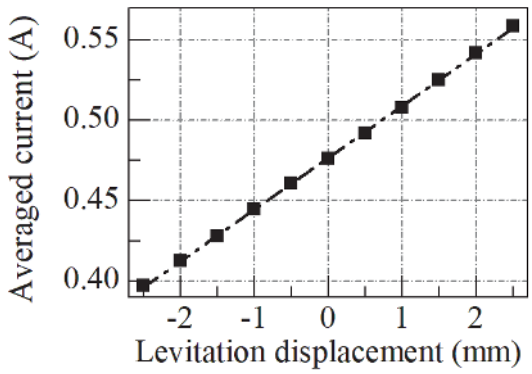

Figure 6.
The maglev system current dynamic in closed loop.

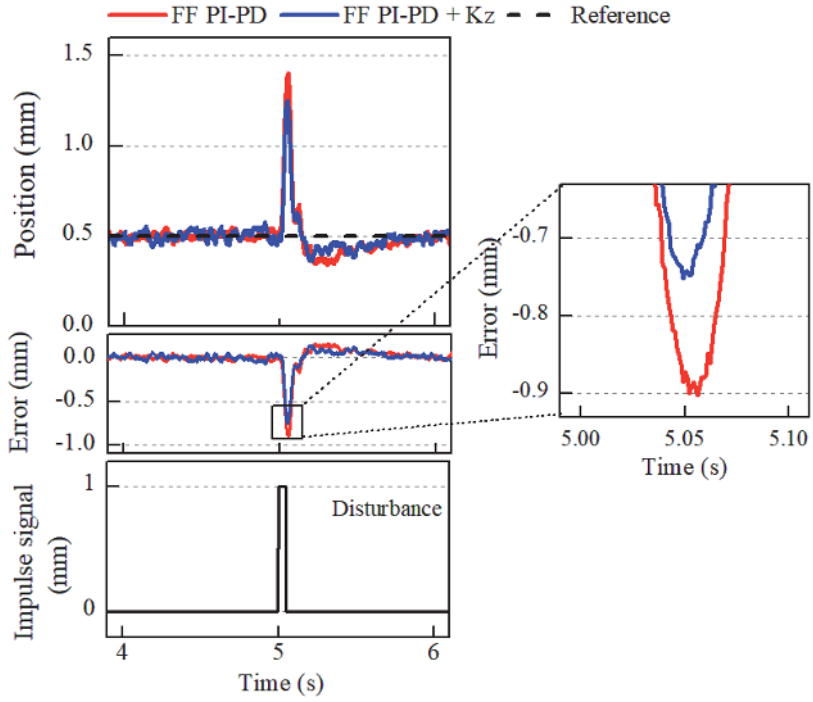

Figure 7.
Experimental impulse disturbance rejection performance.

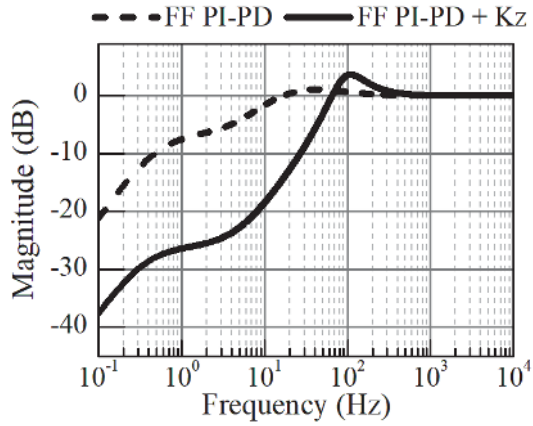

Figure 8.
Simulated frequency response for sensitivity of FF PI-PD and FF PI-PD + Kz controllers.

3.3 Stability analysis

Basically, digital control systems are used for motion control. Thus, the stability of the FF PI-PD + K_z control system is discussed in discrete-time. The nonlinear elements of the controller are undergone linearization and the linearized gains are used for the stability analysis. After linearized, the feedforward and disturbance compensator gains are 0.26 V/mm and 30.67 mm/A, respectively. The stability analysis using the linearized model is adequate to provide the important knowledge of stability. The discrete-time FF PI-PD + K_z control system is illustrated in **Figure 9**.

Using backward difference rule, the pulse transfer function of the FF PI-PD + K_z control system is expressed as

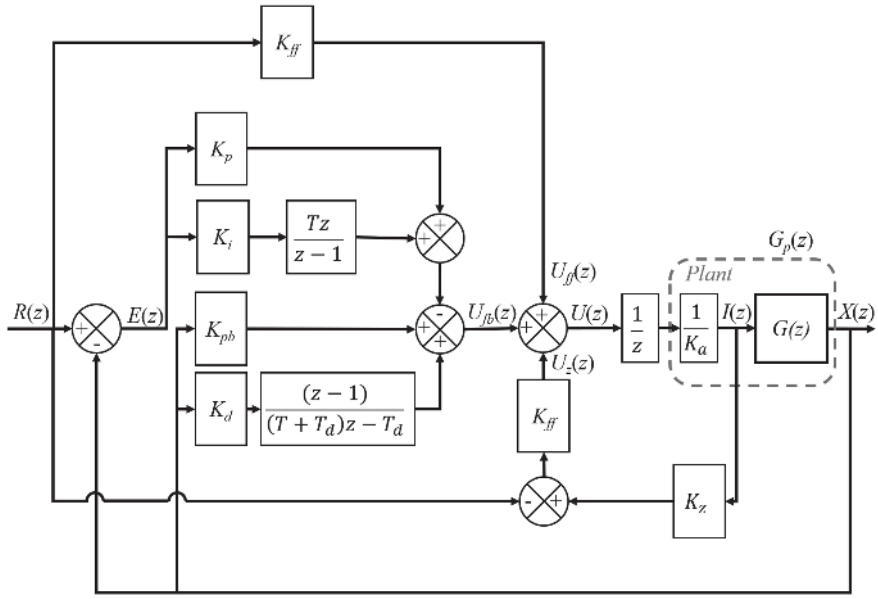

Figure 9.
Discrete-time of FF PI-PD + Kz control system.

$$T(z) = \frac{X(z)}{R(z)} = \frac{z^{-1}G_p(z)G_c(z)}{1 + z^{-1}G_p(z)G_c(z)} \tag{23}$$

where

$$G_p(z) = \frac{\mu_2 z + \mu_3}{z^2 - \mu_4 z + 1}$$

$$G_c(z) = \frac{\mu_5 z^2 + \mu_6 z + \mu_7}{\mu_8 z^2 - \mu_9 z + \mu_{10}}$$

$\mu_1 = \beta/\gamma^2$, $\mu_2 = \mu_1\left(e^{\gamma T} + e^{-\gamma T}\right) - \mu_1 - \frac{\mu_1}{2}\left(e^{\gamma T} + e^{-\gamma T}\right)$, $\mu_3 = -\mu_1 + \frac{\mu_1}{2}e^{\gamma T} + \frac{\mu_1}{2}e^{-\gamma T}$, $\mu_4 = e^{\gamma T} + e^{-\gamma T}$, $\mu_5 = K_i T^2 + \left(K_p - K_{pb} + K_{ff}K_z\right)T + \left(K_p - K_{pb} + K_{ff}K_z\right)T_d + K_i T T_d - K_d$, $\mu_6 = \left(K_{pb} - K_{ff}K_z - K_p\right)T + \left(2K_{pb} - 2K_{ff}K_z - 2K_p\right)T_d - K_i T T_d + 2K_d$, $\mu_7 = \left(K_p + K_{ff}K_z - K_{pb}\right)T_d - K_d$, $\mu_8 = (T + T_d)$, $\mu_9 = T + 2T_d$, $\mu_{10} = T_d$ and T_d = 1.60 × 10^{-3} s.

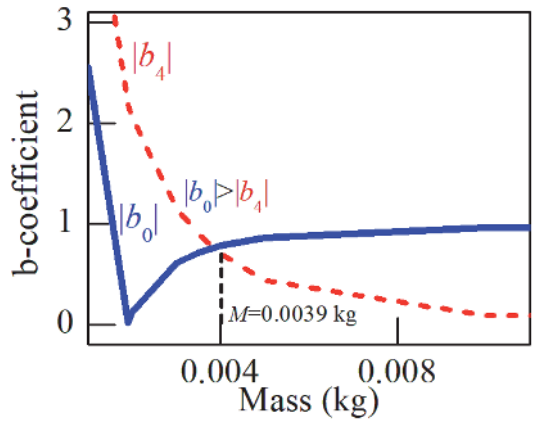

Figure 10.
b-*coefficient of mass parameter variation.*

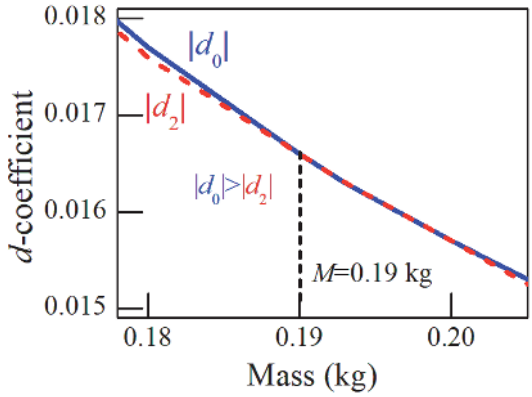

Figure 11.
d-*coefficient of mass parameter variation.*

The Jury stability test is used to examine the stability limit of the FF PI-PD + K_z control system. The characteristic in Eq. (23) is used to identify the stability limit of the FF PI-PD + K_z control system. **Figures 10** and **11** show the minimum and maximum values of the mass parameter variation, respectively. The results show that the parameter that influences the stability of the control system is the object mass, M. To maintain the system stable, the object mass, M must be kept between 3.9 g < M < 190 g. In short, the Jury test proves that the FF PI-PD + K_z control system remains stable with the increment of mass weight to two times of its default one.

4. Experimental performance

Experiments are conducted to evaluate the effectiveness of the FF PI-PD + K_z control system. Two types of motion control that are positioning and tracking controls are experimentally examined. The full-state feedback (FSF) controller is designed and compared with the proposed control. FSF control is chosen for the comparison purpose is because it is an advanced controller that has been regularly applied to the nonlinear applications such as maglev system [18, 19], inverted pendulum system [20] and others. Besides, the FF PI-PD control is compared with the proposed one in order to prove the usefulness of the disturbance compensator. The robust performance of the proposed control is examined by injecting an impulse disturbance to the system, and followed by increasing the mass of the ball by 25%.

Figure 12 illustrates the block diagram of the FSF controller. An integral action is added into the FSF controller to eliminate the steady state error by increasing the transfer function to type one system. From **Figure 12**, the system state-space model is written as

$$\begin{bmatrix} \dot{x}(t) \\ \dot{e}(t) \end{bmatrix} = \begin{bmatrix} A & 0 \\ -C & 0 \end{bmatrix} \begin{bmatrix} x(t) \\ e(t) \end{bmatrix} + \begin{bmatrix} B \\ 0 \end{bmatrix} u(t) + \begin{bmatrix} 0 \\ 1 \end{bmatrix} r(t) \tag{24}$$

where.

$$\mathrm{A} = \begin{bmatrix} 0 & 1 & 0 \\ K_x/M & 0 & -K_c/M \\ 0 & 0 & 0 \end{bmatrix}, \quad \mathrm{B} = \begin{bmatrix} 0 \\ 0 \\ 1/K_a \end{bmatrix} \quad \text{and} \quad \mathrm{C} = [K_s \;\; 0 \;\; 0]$$

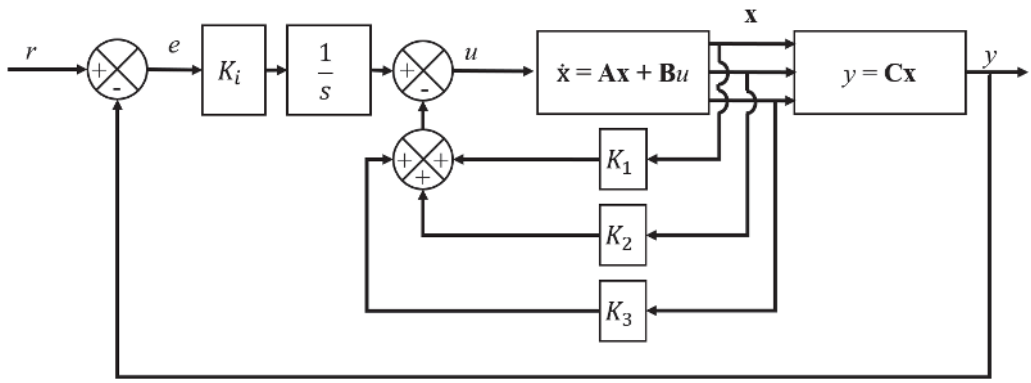

Figure 12.
Block diagram of the full-state feedback (FSF) controller.

Based on Eq. (24), the state feedback control law, $u_{fsf}(t)$ is defined as

$$u_{fsf}(t) = -\mathbf{K}\mathbf{x}(t) + K_i e(t) \tag{25}$$

where **K**, K_i, $x(t)$ and $e(t)$ represent the state feedback gain matrix, integral gain, levitation displacement and error, accordingly.

Ackermann's formula is used to determine the state feedback gain matrix, **K** and the integral gain, K_i. For comparative purpose, the design specifications of FSF controller are set as: settling time, t_s = 0.5 s, percentage of overshoot, $\%OS < 10\%$ as well as third and fourth poles location, α = 10. The frequency of first-order low-pass filter, ω_c is selected based on the system cut-off frequency at around 600 rad/s. The FSF controller parameters are tuned to have the best positioning performance at 1.0 mm step response as similar to the FF PI-PD + K_z controller (see **Figure 13**). **Table 2** shows the controller parameters for FSF, FF PI-PD and FF PI-PD + K_z control systems.

4.1 Positioning performance

In this experiment, the initial position is set at 10.5 mm and the working range is within ±2.5 mm. **Figures 14** and **15** show the experimental positioning performance of the FSF, FF PI-PD and FF PI-PD + K_z control systems to 0.5 mm, 1.0 mm, −0.5 mm and − 1.0 mm step inputs, respectively. As observed clearly, the FF PI-PD + K_z controller shows almost identical positioning performance, with no overshoot as the FF PI-PD and FSF control systems. However, the FSF control system

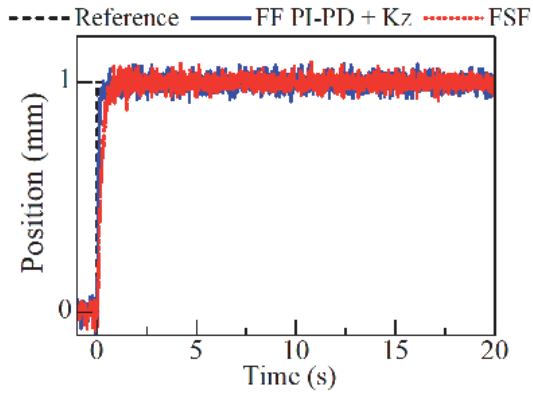

Figure 13.
Experimental step responses of controllers at 1.0 mm reference input.

Controller	K_1	K_2	K_3	K_p	K_i	K_{pb}	K_d
FSF	0.80	0.02	0.01	—	2.36	—	—
FF PI-PD	—	—	—	0.45	1.20	0.15	0.03
FF PI-PD + K_z	—	—	—	0.45	1.20	0.15	0.03

Table 2.
Controller parameters.

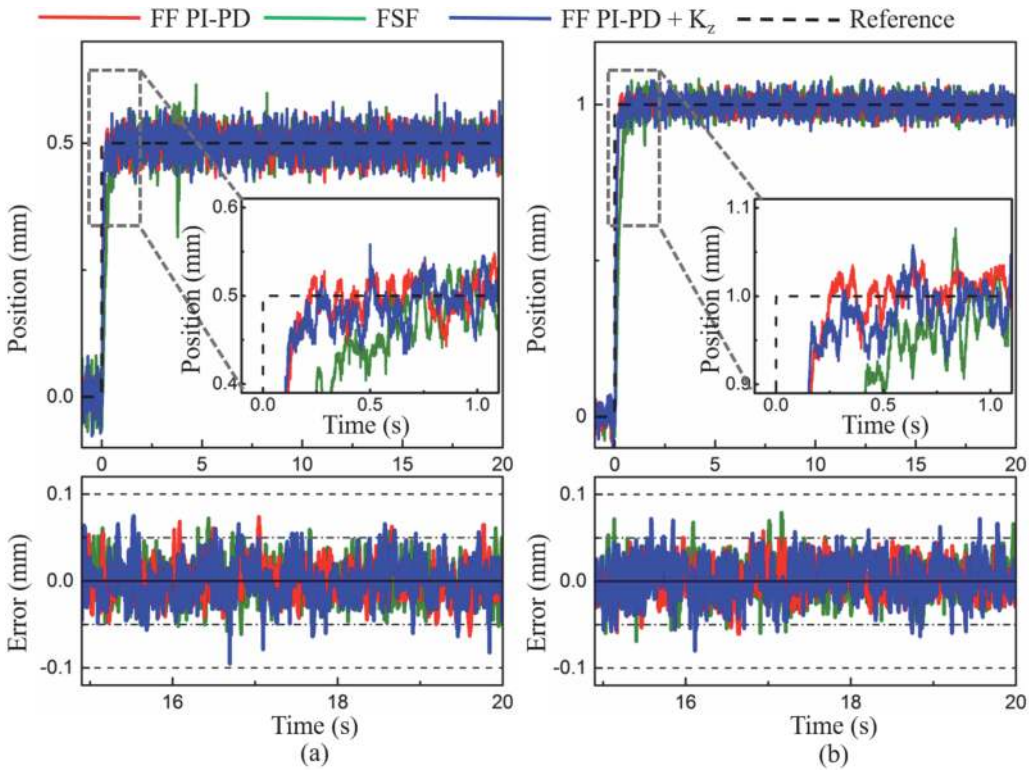

Figure 14.
Experimental step responses of the three control systems at positive side direction. (a) Responses to a 0.5 mm step input (default mass). (b) Responses to a 1.0 mm step input (default mass).

takes longer settling time than the FF PI-PD and FF PI-PD + K_z controllers to reach steady-state that less than ±100 μ m. **Figure 16** presents the simulated closed-loop frequency response for the three control systems. As can be seen in **Figure 16**, the FF PI-PD and FF PI-PD + K_z controls demonstrate wider bandwidth as compared to the FSF control. Therefore, it can be explained that the both FF PI-PD and FF PI-PD + K_z controllers could perform shorter settling time than the FSF controller.

Table 3 shows the quantitative comparison of twenty (20) repeatability experimental results for the point-to-point motion of the three controllers. The settling time, t_s is determined as the time where the system is stabilized within ±100 μm. All three controllers demonstrate zero overshoot at every step input. Although FSF performs zero overshoot in all the step input, it takes long settling time to reach steady state that of less than ±100 μm. The settling time of the FF PI-PD + K_z is 65.6% shorter than the FSF controller.

4.2 Tracking performance

For tracking motion, periodic trapezoidal reference input is utilized to command the maglev system. The maximal tracking error is stated as E_{max} = max $|x_r - x|$ where

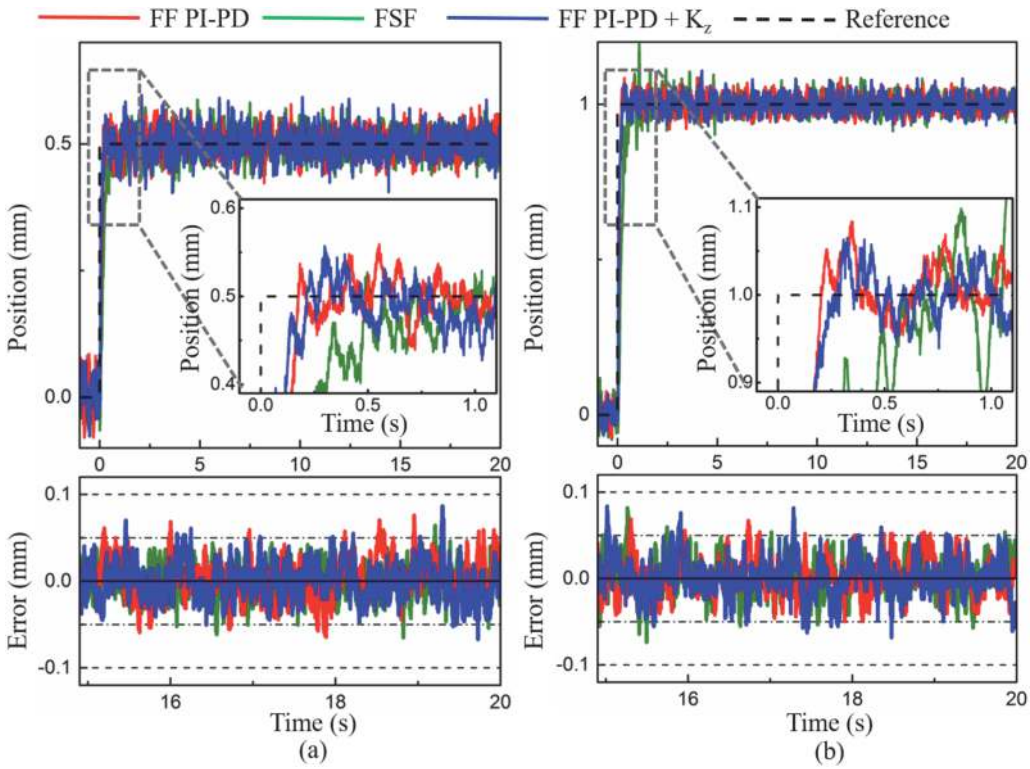

Figure 15.
Experimental step responses of the three control systems at negative side direction. (a) Responses to a − 0.5 mm step input (default mass). (b) Responses to a −1.0 mm step input (default mass).

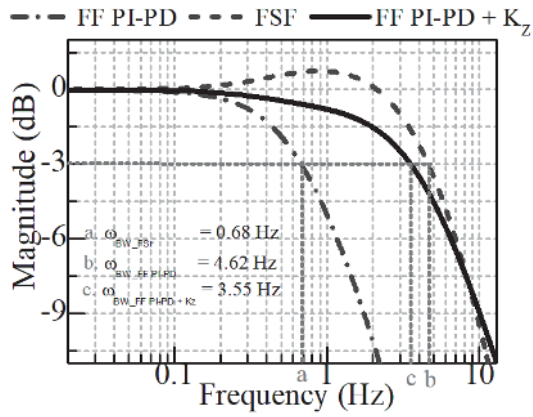

Figure 16.
Simulated closed-loop frequency response.

x_r is the reference input and x is the levitation height. In addition, the root mean square error, E_{rms} is calculated as $\sqrt{1/N\sum_{k=1}^{N}e^2}$ where N represents the number of data samples and e is the tracking error.

Figure 17 illustrates the trapezoidal tracking performance of the FSF, FF PI-PD and FF PI-PD + K_z control systems to 0.5 mm and 1.0 mm amplitudes. Both FF PI-PD and FF PI-PD + K_z controllers demonstrate almost identical tracking performance. The tracking error difference between them is insignificant. On the other hand, the FSF controller demonstrates the worst tracking performance with the largest tracking error among the compared controllers. The maximum tracking

Step height	Performance index		FF PI-PD + K_z	FF PI-PD	FSF
0.5 mm	*OS*, %	Average	0.00	0.00	0.00
		Standard deviation	0.00	0.00	0.00
	t_s, s	Average	1.45×10^{-1}	1.17×10^{-1}	4.35×10^{-1}
		Standard deviation	3.01×10^{-2}	1.91×10^{-2}	6.37×10^{-2}
1.0 mm	*OS*, %	Average	0.00	0.00	0.00
		standard deviation	0.00	0.00	0.00
	t_s, s	Average	2.02×10^{-1}	1.60×10^{-1}	5.48×10^{-1}
		Standard deviation	3.82×10^{-2}	1.19×10^{-2}	5.45×10^{-2}
−0.5 mm	*OS*, %	Average	0.00	0.00	0.00
		Standard deviation	0.00	0.00	0.00
	t_s, s	Average	1.25×10^{-1}	1.90×10^{-1}	3.83×10^{-1}
		Standard deviation	3.22×10^{-2}	1.19×10^{-1}	8.64×10^{-2}
−1.0 mm	*OS*, %	Average	0.00	0.00	0.00
		Standard deviation	0.00	0.00	0.00
	t_s, s	Average	1.77×10^{-1}	2.03×10^{-1}	5.06×10^{-1}
		Standard deviation	2.35×10^{-2}	6.07×10^{-2}	5.36×10^{-2}

OS*: overshoot, t_s: settling time.*

Table 3.
Experimental positioning performances of twenty (20) experiments for three controllers (default mass).

error of the FSF controller at 0.5 mm amplitude is around 1.5 times larger than the FF PI-PD + K_z controller. Meanwhile, as the amplitude increased to 1.0 mm, the FSF controller maximum tracking error is about 2 times larger than the FF PI-PD + K_z controller (see error signal in **Figure 17(b)**). The maximum tracking error occurred at the slope of the trapezoidal signal where the velocity changes. Thus, the experimental results proved that the FSF controller has low adaptability to the velocity change. The FSF controller comprised of narrow bandwidth (see **Figure 16**). Hence, it can explain that the FSF controller does not have sufficient speed to cope with the variation of velocity effectively. The average of E_{max} and E_{rms} values of twenty (20) experiments for the tracking motion is summarized in **Table 4**. At amplitude 0.5 mm, the E_{max} and E_{rms} values of the FSF controller are 48.2% and 46.7% larger than the FF PI-PD + K_z controller. Besides, the E_{max} and E_{rms} values of the FF PI-PD + K_z controller are 47.1% and 58.9% smaller than the FSF controller at 1.0 mm amplitude. On the other hand, the difference of E_{max} and E_{rms} values between the FF PI-PD and the FF PI-PD + K_z controllers are insignificant. Overview, the FF PI-PD and FF PI-PD + K_z control systems track the trapezoidal signal more accurately and precisely with the smaller E_{max} and E_{rms} values as compared to the FSF controller.

4.3 Robustness performance

The robust performance of the proposed controller is evaluated in the presence of mass variation. The 25% extra load is added to the default load of the mechanism. In this experiment, the control performance is examined in two type of motions: point-to-point and tracking motions. The robust performance of the FF PI-PD + K_z controller is then compared with the FF PI-PD and FSF controllers.

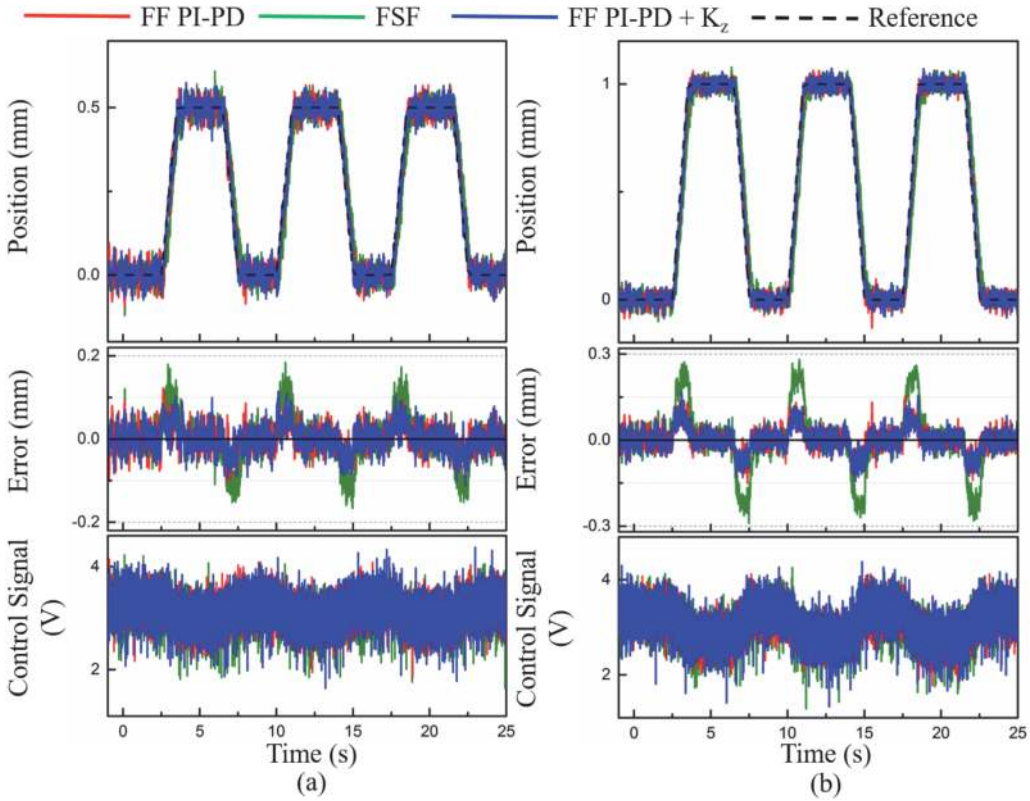

Figure 17.
Comparative experimental trapezoidal tracking responses of the three controllers. (a) Responses to a trapezoidal input: 0.5 mm (default mass). (b) Responses to a trapezoidal input: 1.0 mm (default mass).

Reference input	Controller	E_{max}	E_{rms}
		Average, mm	Average, mm
Trapezoidal, 0.5 mm	FSF	2.28×10^{-1}	5.72×10^{-2}
	FF PI-PD	1.21×10^{-1}	3.04×10^{-2}
	FF PI-PD + K_z	1.18×10^{-1}	3.05×10^{-2}
Trapezoidal, 1.0 mm	FSF	2.95×10^{-1}	1.04×10^{-1}
	FF PI-PD	1.51×10^{-1}	4.24×10^{-2}
	FF PI-PD + K_z	1.56×10^{-1}	4.27×10^{-2}

Table 4.
Average of twenty (20) experiments trapezoidal motion for the three controllers (default mass).

4.3.1 Point-to-point motion

The positioning responses with the increased mass are shown in **Figures 18** and **19**. As the mass is increased, the FF PI-PD controller shows overshoot occurrence at both positive and negative directions. Thus, the FF PI-PD controller fails to demonstrate its robust performance. On the other hand, the FF PI-PD + K_z controller demonstrates high robustness via demonstrating zero overshoot at all the step responses regardless of the variation of mass. Hence, the experimental positioning results proved that the disturbance compensation control scheme is comprised in the FF PI-PD + K_z controller and it has led to the less sensitive to parameter variation characteristic of the controller. Although the FSF controller performs its good robustness through showing

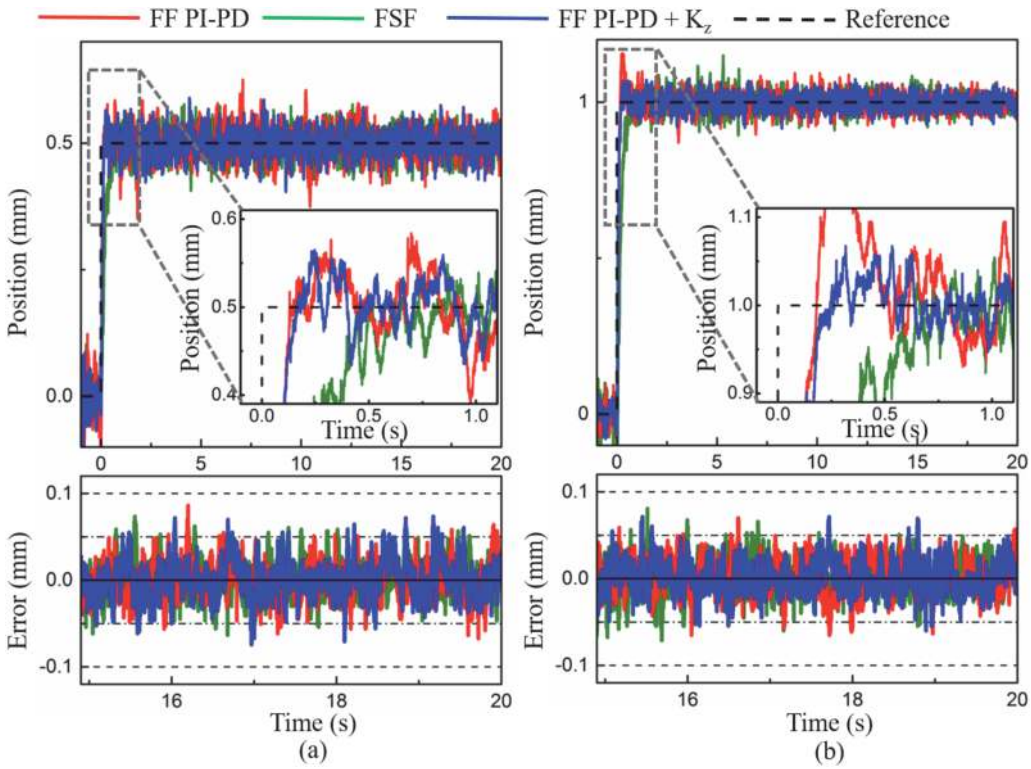

Figure 18.
Experimental step responses of the three control systems at positive side direction. (a) Responses to a 0.5 mm step input (increased mass). (b) Responses to a 1.0 mm step input (increased mass).

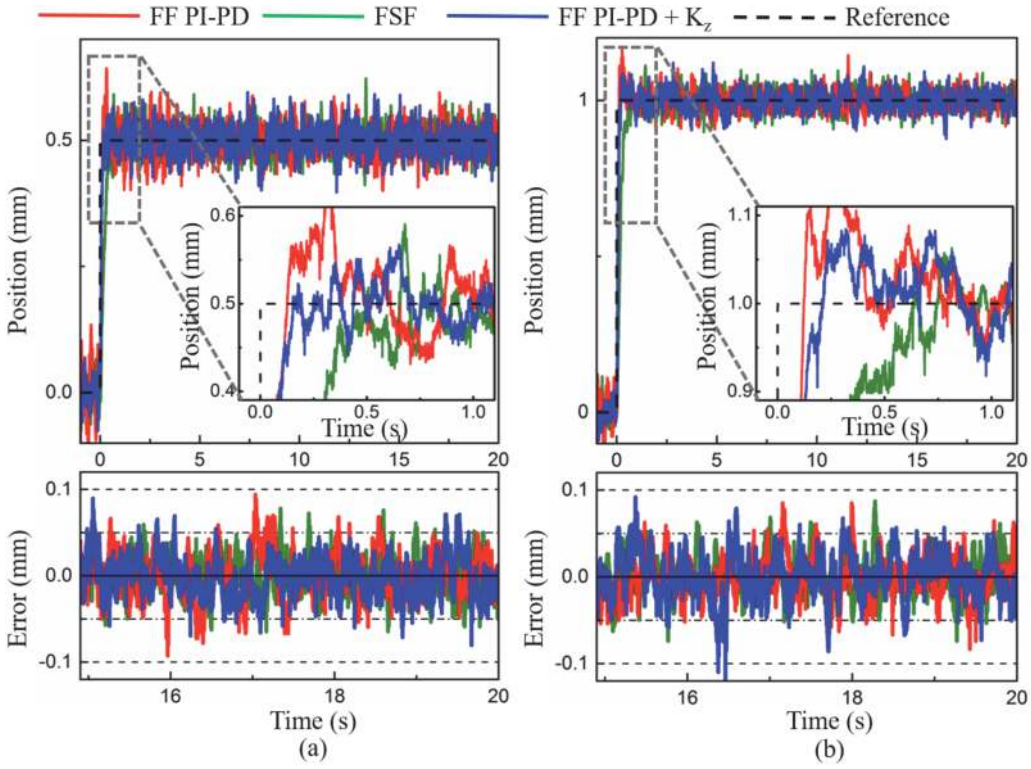

Figure 19.
Experimental step responses of the three control systems at negative side direction. (a) Responses to a −0.5 mm step input (increased mass). (b) Responses to a −1.0 mm step input (increased mass).

zero overshoot at all the step responses, it takes longer positioning time than the FF PI-PD + K_z controller to reach the steady-state (**Table 5**).

Table 6 shows the quantitative comparison of twenty (20) repeatability tests for the point-to-point motion in the presence of mass variation. As can be seen from **Table 6**, when the mass of table is increased, the FF PI-PD controller fails to demonstrate its robustness by producing a large overshoot. The change of mass has caused the overshoot of the FF PI-PD controller is increased by 20% of the default mass condition and the settling time of the FF PI-PD controller is 47.9% longer than the FF PI-PD + K_z controller. In contrast, the FF PI-PD + K_z controller has successfully remained its high robust performance via demonstrating zero overshoot at all the step responses. It is evident that the FF PI-PD + K_z controller enhances the robustness of the FF PI-PD controller via introducing the disturbance compensation

Step height	Performance index		FF PI-PD + K_z	FF PI-PD	FSF
0.5 mm	*OS*, %	Average	0.00	0.00	0.00
		Standard deviation	0.00	0.00	0.00
	t_s, s	Average	1.13×10^{-1}	1.77×10^{-1}	3.92×10^{-1}
		Standard deviation	1.60×10^{-2}	1.05×10^{-1}	1.28×10^{-1}
1.0 mm	*OS*, %	Average	0.00	1.40×10^{1}	0.00
		Standard deviation	0.00	2.52×10^{-2}	0.00
	t_s, s	Average	1.50×10^{-1}	2.95×10^{-1}	5.08×10^{-1}
		Standard deviation	1.47×10^{-2}	9.75×10^{-2}	8.60×10^{-2}
−0.5 mm	*OS*, %	Average	0.00	2.80×10^{1}	0.00
		Standard deviation	0.00	2.85×10^{-2}	0.00
	t_s, s	Average	1.15×10^{-1}	2.77×10^{-1}	3.59×10^{-1}
		Standard deviation	5.40×10^{-2}	1.93×10^{-1}	8.42×10^{-2}
−1.0 mm	*OS*, %	Average	0.00	1.75×10^{1}	0.00
		Standard deviation	0.00	3.66×10^{-2}	0.00
	t_s, s	Average	2.27×10^{-1}	4.32×10^{-1}	4.57×10^{-1}
		Standard deviation	1.17×10^{-2}	4.67×10^{-2}	6.87×10^{-2}

OS*: overshoot, t_s: settling time.*

Table 5.
Experimental positioning performances of twenty (20) experiments for three controllers (increased mass).

Reference input	Controller	E_{max}	E_{rms}
		Average, mm	Average, mm
Trapezoidal, 0.5 mm	FSF	1.92×10^{-1}	5.33×10^{-2}
	FF PI-PD	1.53×10^{-1}	3.50×10^{-2}
	FF PI-PD + K_z	1.26×10^{-1}	3.05×10^{-2}
Trapezoidal, 1.0 mm	FSF	2.99×10^{-1}	9.87×10^{-2}
	FF PI-PD	1.72×10^{-1}	4.04×10^{-2}
	FF PI-PD + K_z	1.57×10^{-1}	3.84×10^{-2}

Table 6.
Average of twenty (20) experiments trapezoidal tracking motion for three controllers (increased mass).

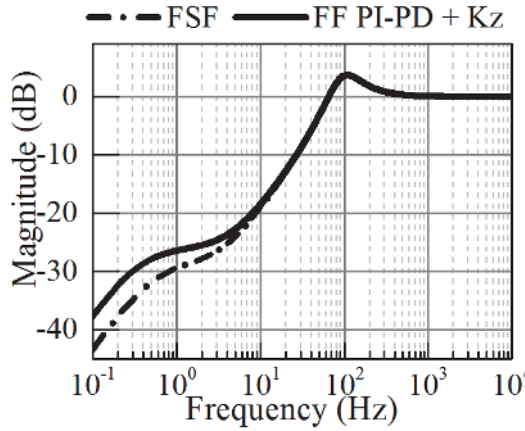

Figure 20.
Sensitivity response of the FF PI-PD + K_z and the FSP controllers.

control scheme. On the other hand, the FF PI-PD + K_z achieves approximately three (3) times shorter settling time than the FSF controller when the mass increased. In short, the FF PI-PD + K_z controller demonstrates the best positioning performance among the compared controllers regardless of the mass variation.

As referred to the **Figure 20**, the FF PI-PD + K_z controller performs smaller sensitivity function magnitude than the FF PI-PD controller. Hence, it is less sensitive to parameter variation. In short, despite the variation of mass and amplitude, the FF PI-PD + K_z controller demonstrates a superior tracking performance than the FF PI-PD and FSF controllers, where it tracks the trapezoidal command accurately and precisely via illustrating the lowest E_{max} and E_{rms} values.

5. Conclusions

In this chapter, the architecture of the FF PI-PD + K_z control system for enhancing the positioning, tracking and robust performances of the maglev system is presented. Initially, a two-degree-of-freedom (2 DOF) PID control – PI-PD, is used to improve the transient response of the conventional PID controller by minimizing the resonance peak. However, the PI-PD control has not sufficiently performed promising positioning responses. A as solution, a model-based feedforward (FF) control is integrated to the PI-PD control for further improving the following characteristic and overshoot reduction capabilities of the mechanism. Lastly, a disturbance compensator (K_z) is served to enhance the system robustness via lowering the sensitivity function magnitude. Although the framework of proposed controller - FF PI-PD + K_z control system is slightly complex than the conventional PID controller, but the design procedure of FF PI-PD + K_z control system remains simple, straightforward, and ease to understand. This advantageous highlight the applicability of the FF PI-PD + K_z control system in the industrial applications. The effectiveness of the proposed controller is evaluated experimentally in point-to-point and tracking motions in comparison to the FF PI-PD and Full State Feedback (FSF) controllers. The robust performance of the controllers is examined in the presence of the mass variations. As an overview, the FF PI-PD + K_z control system performs well in the positioning and robustness performances as compared to the FF PI-PD and FSF controllers. The comparative experimental results are sufficient to prove the contribution of the FF PI-PD + K_z control system in overshoot reduction and robustness enhancement. As for future work, the robustness performance, and the positioning accuracy of the FF PI-PD + K_z control system will be improved.

Acknowledgements

The authors would like to be obliged to Motion Control Research Laboratory, Center for Robotics and Automations, Faculty of Electrical Engineering, Universiti Teknikal Malaysia Melaka for providing the laboratory facilities and equipment support.

Nomenclature

M	steel ball mass
N_w	number of windings
x_o	nominal displacement
i_o	nominal current
K	electromagnetic constant
K_a	power amplifier
K_s	sensor sensitivity
g	gravitational acceleration
F_m	electromagnetic force
F_g	gravitational force
i	current
x	displacement
g	gravitational acceleration
K_c	current coefficient
K_x	position coefficient
β	open loop gain
γ	open loop pole
α	third pole location
ζ	desired damping ratio
ω_n	desired natural frequency
K_p	proportional gain
K_i	integral gain
K_d	derivative gain
K_{pb}	feedback proportional gain
K_{ff}	linearized feedforward gain
K_z	linearized disturbance compensation gain
δ_{PID}	closed loop PID control characteristic equation
$\delta_{PI\text{-}PD}$	closed loop PI-PD control characteristic equation
$\delta_{desired}$	desired characteristic equation
G_p	plant model
G_{ff}	model-based feedforward control
$G_{PI\text{-}PD}$	PI-PD control
G_z	disturbance compensator
T	sampling time
T_d	time constant of derivative elements with filter
ω_c	system cutoff frequency
$\mathbf{K}$	state feedback gain matrix
u_{fb}	feedback control signal
u_{ff}	feedforward control signal
u	summation signals of u_{fb} and u_{ff}
N	number of data sample
e	tracking error

DOI: http://dx.doi.org/10.5772/intechopen.96769

x_r	reference input
E_{max}	maximal error
E_{rms}	root mean square error

Author details

Shin-Horng Chong*, Roong-Soon Allan Chan and Norhaslinda Hasim
Faculty of Electrical Engineering, Centre for Robotics and Industrial Automation, Universiti Teknikal Malaysia Melaka, Durian Tunggal, Malaysia

*Address all correspondence to: horng@utem.edu.my

References

[1] Yaghoubi H. The most important maglev applications. Journal of Engineering. 2013; 1:19. DOI: https://doi.org/10.1155/2013/537986

[2] Banerjee S, Prasad D, Pal J. Large gap control in electromagnetic levitation. The Instrumentation, Systems, and Automation Society. 2006;45(2): 215-224. DOI: https://doi.org/10.1016/S0019-0578(07)60191-8

[3] Banerjee S, Prasad D, Pal J. Design, implementation and testing of a single axis levitatin system for suspension of a platform. ISA Transactions. 2007;46(2): 239-246. DOI: https://doi.org/10.1016/j.isatra.2006.09.001

[4] Fujimoto K, Sugie T. Freedom in coordinate transformation for exact linearization and its application to transient behavior impovement. Automatica. 2001;37(1): 137-144. DOI: https://doi.org/10.1016/S0005-1098(00)00134-5

[5] Cho D, Kato Y, Darin S. Sliding mode and classical control magnetic levitation system. IEEE Control Systems. 1993;13(1): 42–48. DOI: 10.1109/37.184792

[6] Sinha PK, Pechev AN. Nonlinear H-infinity controllers for electromagnetic suspension systems. IEEE Transactions on Automatic Control. 2004;49(4): 563–568. DOI: 10.1109/TAC.2003.822865

[7] Yang J, Zalotas A, Chen WH, Michail K, Li S. Robust control of nonlinear maglev suspension system with mismatched uncertainties via DOBC approach. ISA Transactions. 2011;50(3): 389-396. DOI: https://doi.org/10.1016/j.isatra.2011.01.006

[8] Yang ZJ, Tateshi M. Adaptive robust nonlinear control of a magnetic levitation system. Automatica. 2001;37(7): 1125-1131. DOI: https://doi.org/10.1016/S0005-1098(01)00063-2

[9] Bächle T, Hentzelt S, Graichen K. Nonlinear model predictive control of a magnetic levitation system. Control Engineering Practice. 2013;21(9): 1250-1258. DOI: https://doi.org/10.1016/j.conengprac.2013.04.009

[10] Qin Y, Peng H, Zhou F, Zeng X, Wu J. Nonlinear modeling and control approach to magnetic levitation ball system using functional weight RBF network-based state dependent ARX model. Journal of the Franklin Insitute. 2015;352(10): 4309-4338. DOI: https://doi.org/10.1016/j.jfranklin.2015.06.014

[11] Klau M, Kalúz M, Kvasnica M. Real-time implementation of an explicit MPC-based reference governor for control of a magnetic levitation system. Control Engineering Practice. 2017;60: 99-105. DOI: https://doi.org/10.1016/j.conengprac.2017.01.001

[12] Golob M, Tovornik B. Modeling and control of the magnetic suspension system. ISA Transactions. 2003;42: 89-100. DOI: https://doi.org/10.1016/S0019-0578(07)60116-5

[13] Chen SY, Lin FJ, Shyu KK. Direct decentralized neural control for nonlinear MIMO magnetic levitation system. Neurocomputing. 2009;72(13): 3220-3230. DOI: https://doi.org/10.1016/j.neucom.2009.02.009

[14] Leva A, Bascetta L. Designing the feedforward part of 2-dof industrial controllers for optimal tracking. Control Engineering Practice. 2007;15(8): 909-921. DOI: https://doi.org/10.1016/j.conengprac.2006.11.009

[15] Ghosh A, Krishnan TR, Tejaswy P, Mandal A, Pradhan JK, Ranasingh S. Design and implementation of a 2-dof PID compensation for magnetic levitation systems. ISA Transactions. 2014;53(4): 1216-1222. DOI: https://doi.org/10.1016/j.isatra.2014.05.015

[16] Soon ACR, Chong SH, Said MA. 2-dof lead-plus-PI control approach for magnetic levitation system. Journal of Telecommunications, Electronic and Computer Engineering. 2016;8(11): 3–8.

[17] Soon ACR, Chong SH, Said MA. Position control of a magnetic levitation system via a PI-PD control with feedforward compensation. In: Proceedings of the 56th Annual Conference of the Society of Instrumentation and Control Engineers of Japan (SICE'17): 19–22 September 2017; Kanazawa, Japan: IEEE; 2017. p. 73–78

[18] Schuhmann T, Hofmann W, Werner R. Improving operational performance of active magnetic bearings using kalman filter and state-feedback control. IEEE Transactions on Industrial Electronics. 2012;59(2): 821–829. DOI: 10.1109/TIE.2011.2161056

[19] Wiboonjaroen W, Sujitjorn S. Stabilization of a magnetic levitation control system via state-PI feedback. International Journal of Mathematical Models and Methods in Applied Sciences. 2013;7(7): 717–727.

[20] Tang TF, Chong SH, Pang KK. Stabilization of a rotary inverted pendulum system with double PID and LQR control: experimental verification. International Journal of Automation and Control. 2020;14(1): 18-33. DOI: https://doi.org/10.1504/IJAAC.2020.103799